PLASMA ACCELERATORS

T. Katsouleas, C. Joshi, J.M. Dawson, F.F. Chen, C. Clayton,
W.B. Mori, C. Darrow, D. Umstadter
University of California, Los Angeles, CA 90024

ABSTRACT

We review the progress made on several schemes for acceleration in a plasma medium. The beat wave accelerator is becoming fairly well developed with recent advances made on theoretical, computational, and experimental fronts. Progress on three new concepts, the surfatron, the plasma wakefield, and the plasma grating or rippled plasma accelerator is also described.

INTRODUCTION

The first question one might ask when considering a plasma as a medium for supporting large amplitude electric fields for particle acceleration is "Why use a plasma?" In light of their history of unexpected instabilities and complexity, plasmas may seem an unlikely path toward the goal of high gradient particle accelerators. In this paper, the results of investigations of plasma as a medium for high-gradient acceleration are presented. Recent work demonstrates that plasma properties are somewhat desirable and often unavoidable when contemplating advanced accelerator concepts.

As a first step toward addressing the question of why accelerate in plasma, let us briefly examine some alternatives. Conventional accelerators can be expected to produce accelerating gradients of the order 20-100 MeV/m. At field strengths not too much higher, the problem of breakdown in the accelerator walls arises. Similarly, many of the near field laser schemes considered at this conference will unintentionally become plasma schemes if the laser intensity is too high. This suggests the first advantage of a plasma accelerator: it is already fully ionized and cannot be destroyed any more than it already is.

Next, one might look to high powered lasers with fields as high as 5 GeV/cm[1] to directly accelerate particles. However, the laser fields are transversely polarized and coupling to these fields (the far field schemes) necessarily leads to transverse particle acceleration and radiation losses. Some direct acceleration in the longitudinal direction is possible from the radiation pressure of the light[2]. However, for a relativistic particle this force decreases as one over the Lorentz factor γ of the particle[3].

On the other hand, the accelerating force of a longitudinal electric field is invariant under Lorentz transformations to any frame moving along the field direction. Hence, the second advantage of a plasma accelerator: plasmas are capable of supporting large,

longitudinal electric field waves (i.e., space charge waves for which the wavenumber k is parallel to the electric field E).

We can estimate just how large the plasma wave fields can be from Poisson's equation:

$$\nabla\cdot\vec{E} = 4\pi e\,\delta n_e \qquad (1)$$

where δn_e is the perturbed electron density of the plasma and the ion background is assumed uniform and immobile. Now the largest density compression or rarefaction that can occur is when all of the plasma electrons are removed. In that case $\delta n_e \simeq n_o$, the equilibrium density. Assuming a plasma wave with phase velocity near c and frequency near the plasma frequency $\omega_p = (4\pi n_o e^2/m_e)^{1/2}$ so that $k \approx \omega_p/c$ and approximating $\nabla\cdot E \sim ikE$, we obtain from (1) the maximum electric field amplitude[4]:

$$eE_{MAX} \sim \frac{4\pi n_o e^2}{(\omega_p/c)} = m_e c\omega_p \approx .97\sqrt{n_o}\ \ \mathrm{eV/cm} \qquad (2)$$

This is sometimes referred to as the cold wavebreaking field because it is the amplitude at which a cold plasma wave steepens and becomes double valued so that the crest begins to fall into the trough[5]. This field can be quite large. For example, in a plasma of density $n_o = 10^{18}\mathrm{cm}^{-3}$ the cold wavebreaking field is of the order 1GeV/cm, or about one thousand times the gradient of conventional linacs.

One might be concerned that a medium such as a dense plasma would interfere with the acceleration process via Coulomb scattering or Cerenkov radiation. The dominant energy loss mechanism for electrons above a few MeV is due to multiple scattering from plasma nuclei. Since the radiation length $(-U/[\partial U/\partial x])$ in a hydrogen plasma of density $10^{20}\mathrm{cm}^{-3}$ is roughly 2km[6] and the scattering cross section decreases as energy squared, this should not pose a problem. Furthermore, collisional damping of the laser scales as one over laser intensity to the three halves and is minimal for intense lasers.

Having illustrated two principal advantages of plasma accelerators--immunity from breakdown and potential for large longitudinal electric fields--we turn to describing the progress that has been made toward realizing this potential.

In section I we review the state of understanding of the most developed of the plasma wave excitation schemes: plasma wave generation by the beating of two lasers[7]. Since the first workshop[8], advances have been made on theoretical modelling and two-dimensional computer modelling, and a conclusive experimental demonstration of the plasma beat wave has been performed.

In Section II we examine two mechanisms for particle acceleration in the fields of high-phase velocity plasma waves: the simple beat wave acceleration mechanism and the Surfatron mechanism (using an imposed DC magnetic field).

In Section III we explore two recently proposed plasma wave excitation schemes: the plasma wakefield accelerator[9] and a plasma grating accelerator[10]. The plasma wakefield scheme employs the electron bunches of a conventional accelerator as the free energy source to drive plasma waves which can then be used to further accelerate a trailing bunch of electrons. The plasma grating scheme employs a single laser injected from the side and couples energy to a longitudinal plasma wave via a plasma density ripple (or ion acoustic wave).

In Section IV we summarize the recent progress and discuss plans for a proof of principal 100MeV beat wave accelerator experiment.

I. PLASMA WAVE EXCITATION BY BEATING LASERS

A. THEORETICAL MODELS

The basic mechanism for excitation for a longitudinal plasma wave by laser light is illustrated in Fig. 1.

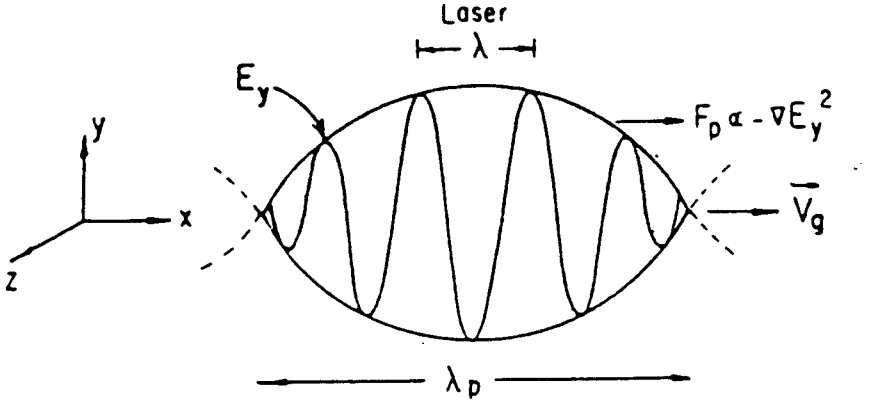

Fig. 1 The radiation pressure or pondermotive force of a packet of light drives longitudinal oscillations of plasma electrons.

Consider a packet of incident electromagnetic radiation which might be created in one of the following two ways: (1) a very short pulse from a single laser (wake plasmon excitation) or (2) by the beat envelope of two lasers of slightly different frequency (beat wave excitation). The packet of radiation exerts a force per unit area on the plasma which is given by the gradient of the stress tensor[11]:

$$F_p \approx \nabla\cdot\vec{\vec{T}}_p - \nabla\cdot\vec{\vec{T}}_v \approx \frac{\varepsilon-1}{8\pi}\frac{\partial}{\partial x}E_y^2 \qquad (3)$$

where $\vec{\vec{T}}_p$, $\vec{\vec{T}}_v$ refer to the stress tensor in plasma and vacuum, respectively, ε is the dielectric function of the plasma ($\varepsilon = 1 - \omega_p^2/\omega^2$, ω is laser frequency and $\omega >> \omega_p$), $\partial/\partial x$ describes

the gradient of the envelope of the packet and E_y is the laser electric field. Since we want just the force on the plasma, we subtracted $\bar{\bar{T}}_v$, the component $\bar{\bar{T}}$ which would exist even if there were no plasma. This so called pondermotive force displaces plasma electrons and creates a temporary charge imbalance in the plasma (the plasma ions are too massive to respond with the electrons). After the packet passes, the space charge force acts to restore the plasma electrons leading to oscillations in the $\hat{x}$ direction and and hence a longitudinal electric field wave.

In the first scenario of a very short pulse, known as the wake plasmon excitation scheme, there is no resonant interaction with the plasma and the plasma essentially receives only a single kick. As a result, the electric force of the plasma wave can never exceed the pondermotive force of the laser. Furthermore, all of the energy required for a full stage of the accelerator must be contained in a single pulse shorter than a plasma period. For a $10^{16}cm^{-3}$ density plasma, the pulse must be 1 picosecond or less. Nevertheless, a short pulse laser with normalized electric field amplitude $V_{osc}/c \equiv eE/m\omega_p c$ of order one has sufficient pondermotive force to create a plasma wave near the cold wavebreaking amplitude (Eq. 2).

In the second scenario involving the beat of two lasers, the plasma wave can be built up resonantly over many plasma periods if the beat frequency of the lasers coincides with the natural frequency at which the plasma electrons oscillate (i.e., $\omega_1 - \omega_2 \approx \omega_p$). In this way, even relatively small laser fields can lead to very large longitudinal plasma wave fields.

Consider the resonant beat wave excitation scheme. By energy and momentum conservation of the laser photons and the plasmon, we have that

$$\omega_1 - \omega_2 = \omega_p \qquad (4)$$

$$k_1 - k_2 = k_p$$

If the plasma is very underdense, such that $\omega_1 \approx \omega_2 >> \omega_p$, we find that the phase velocity of the plama waves is

$$V_{ph} \equiv \frac{\omega_p}{k_p} = \frac{\omega_1 - \omega_2}{k_1 - k_2} = \frac{\Delta\omega}{\Delta k} \approx \frac{\partial\omega}{\partial k} = V_g^{light} = c\,(1 - \omega_p^2/\omega^2)^{1/2} \qquad (5)$$

Thus, the phase velocity of the plasma waves equals the group velocity of the light. The light pulse and the wake of excited plasma waves move as a unit into undisturbed plasma as depicted in Fig. 2.

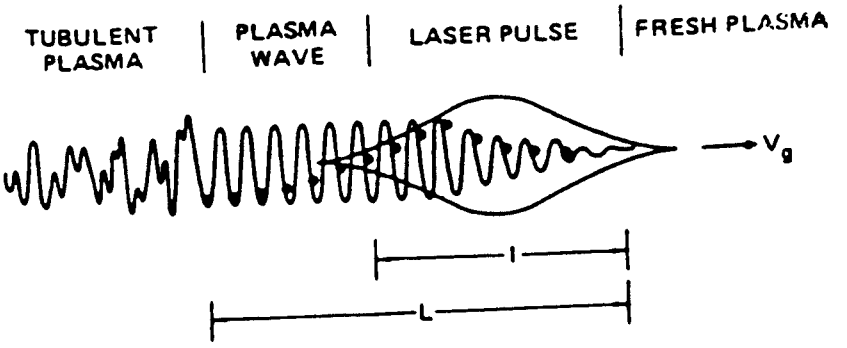

Fig. 2 The laser pulse, the wake of plama waves and the accelerating particles move together at Vg ≈ c into fresh plasma in the beat wave excitation scheme.

If the laser frequencies are much higher than ω_p (i.e., a very underdense plasma), then V_{ph} is very close to c and injected relativistic particles may stay in phase with the electric field of the plasma wave for a sufficient distance to be accelerated to high energy.

As illustrated in the figure, the plasma waves well behind the light pulse become turbulent. This can be due to competing instabilities, such as parametric decay (the decay of an electron plasma wave into a secondary plasma wave and an ion acoustic wave), or as we will discuss shortly, due to relativistic effects which detune the plasma wave frequency from the laser beat frequency. The onset of turbulence does not affect the acceleration of the particles trapped in plasma waves nearer to the light pulse since these continually move into fresh plasma. The onset of turbulence does limit the number of plasma waves that can be used for particle acceleration. For example, if turbulence first onsets due to ion instabilities which grow on a time scale characterized by the ion plasma period ($\tau_i = 2\pi/\omega_{pi}$, $\omega_{pi} = (4\pi ne^2/M_i)^{1/2}$, where M_i is the ion mass), then plasma waves can be created for a time $2\pi/\omega_{pi}$ or a distance $2\pi c/\omega_{pi}$ behind the laser pulse. For a hydrogen plasma this corresponds to 43 ($=\sqrt{M_i/m_e}$) electron plasma wave periods. Plasma waves further than 43 plasma wavelengths behind the laser will begin to become degraded and will probably not be suitable for acceleration.

The growth of the plasma waves behind the laser pulse can be quantified by considering the oscillation of a single background plasma electron driven by the pondermotive force F_p (from Eq. 3 divided by n_o to get the force on a single electron) of the beating lasers:

$$\frac{d}{dt}(\gamma V_x) + \omega_p{}^2 x = \frac{e^2}{2m\omega^2_{1,2}} \Delta k E_1 E_2 \sin(\Delta\omega t - \Delta k x) \qquad (6)$$

where $E_{1,2}$ are the electric field amplitudes of each laser, $\Delta\omega$ and Δk are the beat frequency and beat wave number of the lasers (i.e., $\Delta\omega = \omega_1 - \omega_2 \approx \omega_p$), $\gamma = (1 - V_x^2/C^2)^{-1/2}$, and x is the displacement of the electron from its equilibrium position (i.e., the Lagrangian coordinate). Neglecting the factor γ, this is a simple harmonic oscillator equation with a resonant driver if the beat frequency $\Delta\omega = \omega_p$.

Now the amplitude of the electron's oscillation is proportional to the amplitude E_p of the plasma wave field that its motion supports (the coefficients of proportionality are[12] $\Delta kx = eE_p/m\omega pc \equiv \varepsilon$). Thus, renormalizing the equation, applying the chain rule to γV and expanding γ for small V/c, we obtain the equation for the beat driven plasma wave field normalized to the wavebreaking plama wave amplitude:

$$\ddot{\varepsilon} + \omega_p^2(1 - 3/2\dot{\varepsilon}^2)\varepsilon \approx \frac{\alpha_1\alpha_2}{2} \sin \Delta\omega t \tag{7}$$

Here $\alpha_{1,2} \equiv eE_{1,2}/m\omega_{1,2}c$. This is the model of Rosenbluth and Liu[13] which includes a correction of the plasma frequency due to the relativistic mass increase of the oscillating plasma electrons. Initially, if $\Delta\omega = \omega_p$, the plasma wave amplitude exhibits secular growth

$$\varepsilon(t) = \frac{\alpha_1\alpha_2}{4}\,\omega_p t \tag{8}$$

where ε is now understood to represent the amplitude of the plasma wave. As ε grows, the effective plasma frequency becomes[13] $\omega_{ef} \approx \omega_p(1 - 3\varepsilon^2/16)$. At a time t such that $\int^t(\Delta\omega - \omega_{ef})\,dt' = \pi/2 \approx \omega_p \int 3/16\ \varepsilon^2(t')dt'$, the driver has become $\pi/2$ out of phase with the oscillator and actually begins to drive the oscillation back down. Solving for the value of ε from (8) at this time gives $\varepsilon_{max} = (2\pi\alpha_1\alpha_2)^{1/3}$. A more careful solution of the model equation (7) gives the maximum value of ε as[13]

$$\varepsilon_{max} = \left(\frac{16}{3}\,\alpha_1\alpha_2\right)^{1/3} \tag{9}$$

In principal, Eq. (9) is only valid for $\alpha, \varepsilon << 1$, but simulations indicate that it is a good approximation for values of ε as high as 0.8.

In order to model the rise time of the lasers, we modify the Rosebluth and Liu model (7) slightly by allowing the normalized laser amplitudes $\alpha_{1,2}$ to be functions of time. This leads to modified expressions for growth and saturation:

$$\varepsilon(t) = \int_0^t \frac{\alpha_1(t)\ \alpha_2(t)}{4}\,d\omega_p t \tag{8b}$$

$$\epsilon_{max} = \left(\frac{16}{3}\alpha_1(\tau)\alpha_2(\tau)\right)^{1/3} \qquad (9b)$$

where τ is the value of t at which (8b) and (9b) become equal. Fig. 3 shows a numerical solution of the modified model equation (7) with the analytic expressions corresponding to Eqs. (8b) and (9b) plotted. Given the details of the laser pulse, Eqs. (8b) and (9b) enable predictions for the time for growth and the saturated amplitude of the resulting plasma space charge wave.

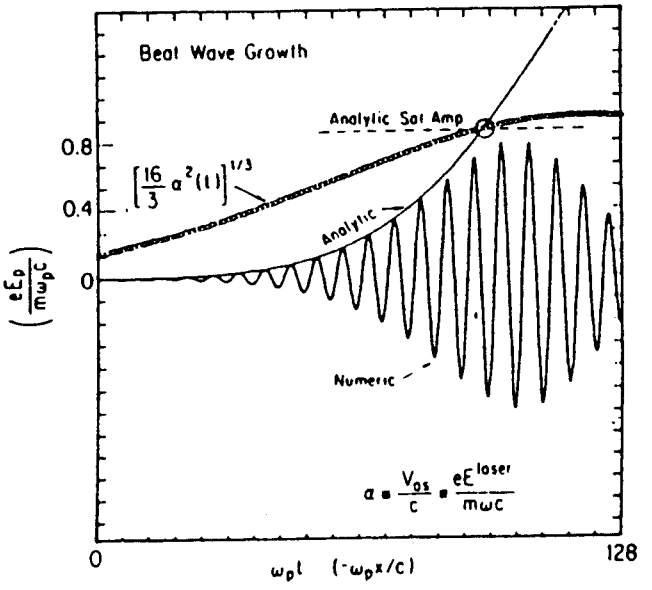

Fig. 3 Numerical solution of the modified plasma beat wave model equation (7) and the corresponding analytic growth and saturation for (8b) and (9b).

In order to minimize the effect of the detuning between the driving frequency $\Delta\omega$ and the effective plasma frequency ω_{ef}, C.M. Tang, et al.[14] have considered altering the beat frequency. They find that the beat wave growth is optimal for

$$\Delta\omega = \omega_p \left[1 - \frac{1}{2}(9\alpha_1\alpha_2/8)^{2/3}\right] \qquad (10)$$

with corresponding maximum amplitude

$$\epsilon_{max} \approx 4\ (\alpha_1\alpha_2/3)^{1/3} \qquad (11)$$

an increase of about 50%. For lasers of $V_{osc}/c \equiv a = .1$, Eq. (10) corresponds to a 2% shift in the laser beat frequency below the natural plasma frequency.

The results of Tang, et al., also provide a guideline for plasma homogeneity requirements. Eq. (10) suggests not only the optimal detuning, but also a scaling law for the fractional density change ($\delta n/n \sim \delta\omega^2_p/\omega^2_p \sim 2\delta\Delta\omega/\omega_p$) that will not have a significant effect on beat wave growth. We might expect to have to maintain the plasma homogeneity to within

$$\frac{\delta n}{n} \sim (\alpha_1\alpha_2)^{2/3} \tag{12}$$

or about 5% for lasers of $V_{osc}/c = .1$. The effect of noise in the plasma density is considered by Horton and Tajima[15], who give conditions for the resonant noise components moving with the beat wave to limit growth of the plasma wave.

B. COMPUTER MODELLING

There are a multitude of mechanisms which might cause the behavior of a real plasma to deviate from the simple model of Eq. (7). Some of these are non-linear wave steepening, thermal corrections, and ion effects. Fully self-consistent particle simulations have been invaluable in separating out the most important effects. In Fig. 4, we show the results of a 1-D simulation in which beating lasers were injected from the right[16]. In (a), the beat pattern of the rising lasers is visible and in (b), we see the characteristic growth and saturation of the plasma space charge wave. Remarkably, Fig. (4b) agrees almost identically with the numerical solution to the model Eq. (7) shown below it. This is true despite the fact that the saturation amplitude is more than 70% of the cold wavebreaking maximum. Many of the non-linear effects associated with particle trapping one normally expects at such amplitudes simply do not appear because the plasma wave phase velocity is too high to allow trapping of the background particles. Only particles with velocity V such that $V/c \gtrsim 1 - \varepsilon - 1/\gamma_{ph}$ can be trapped (see Eq. 19).

Recently, the computer models have been extended to two dimensions[17,18], and a sampling of these results are shown in Figs. 5-7. The 2-D simulations are consistent with the 1-D results and provide insight into transverse properties, such as filamentation and self-focusing.

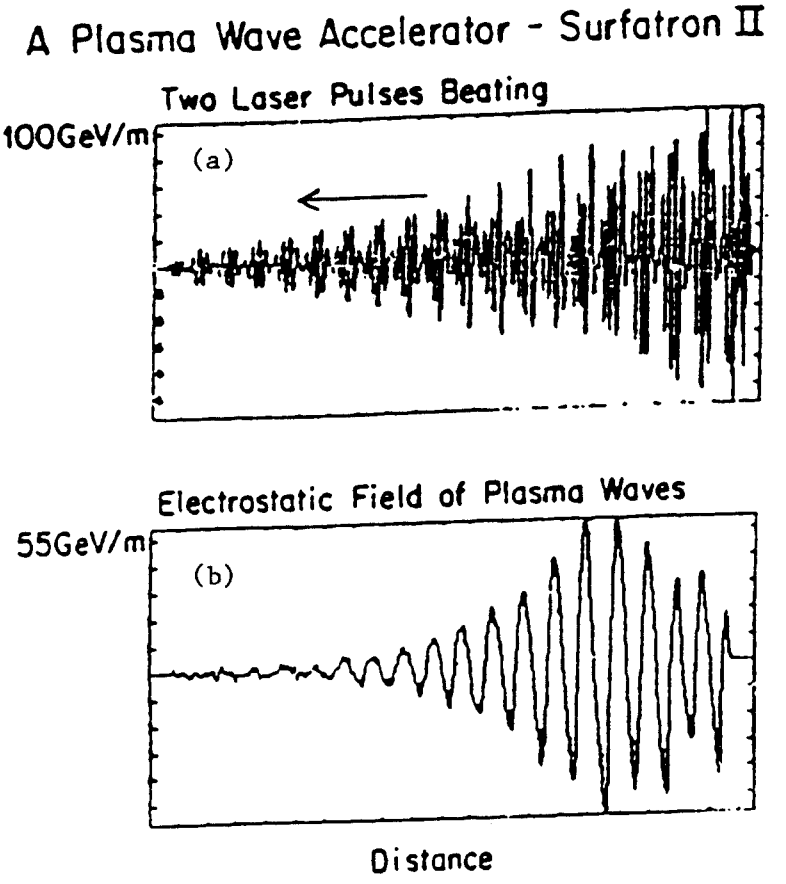

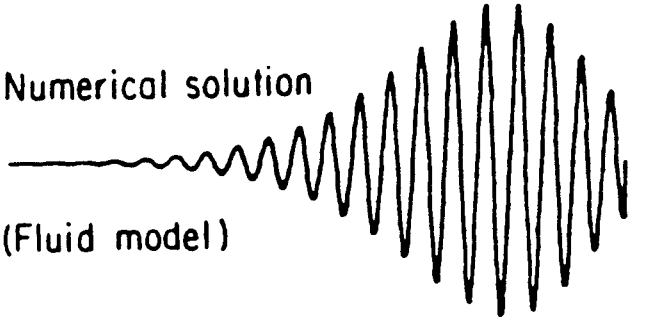

Fig. 4 1-D simulation showing (a) the laser beat pattern, (b) the space charge plasma wave. The numerical solution of the modified fluid model is shown below. $\omega_1=4\omega_p, \omega_2=5\omega_p, \alpha_1=\alpha_2$.

The 2-D contour plot in Fig. 5 shows the generation of coherent plane wave fronts (moving left to right). A slice down the axis, Fig. 5b, shows the growth of the beat wave to be in nice agreement with both the model of section A and the 1-D simulations.

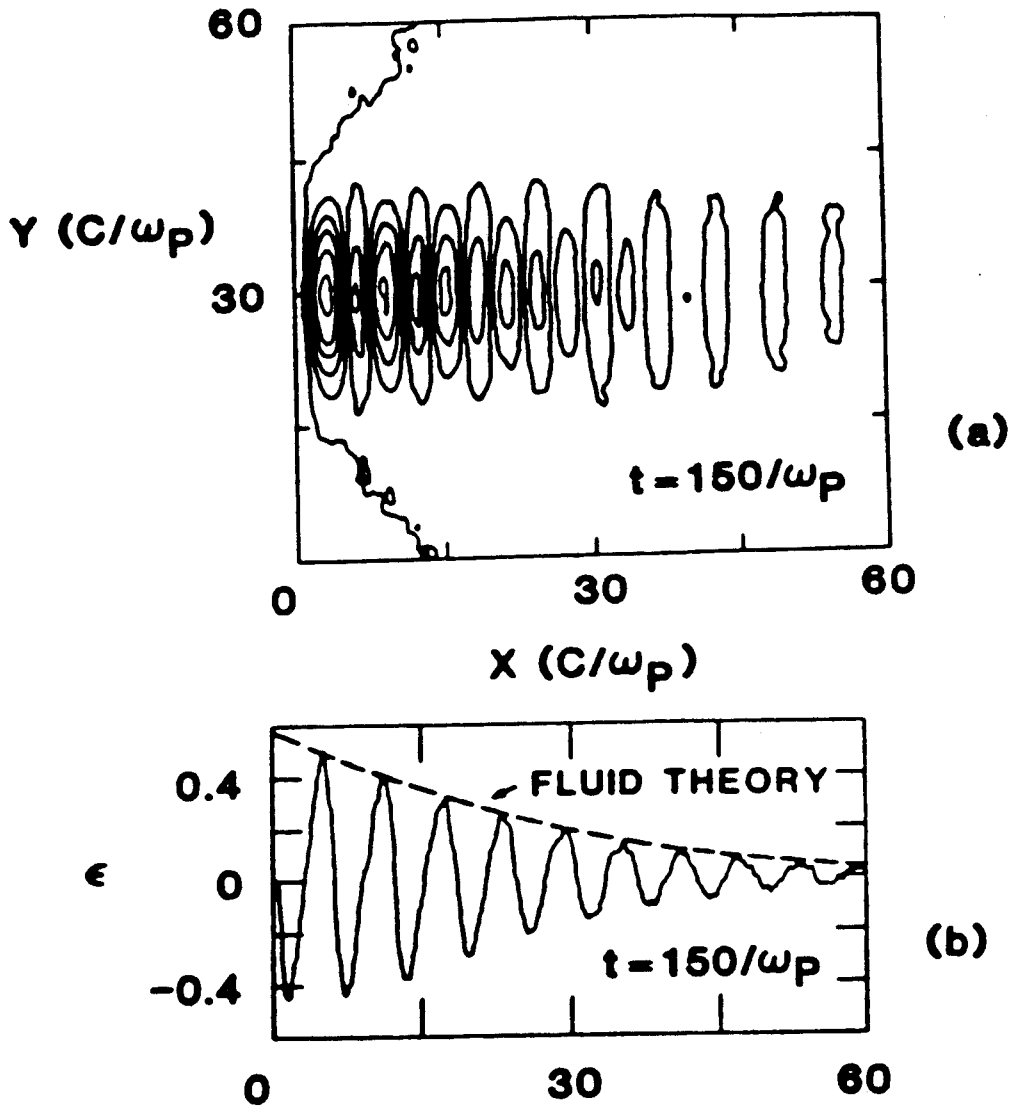

Fig. 5 2-D simulation (a) contour plot of the beat wave and (b) a slice down the y-30 axis.

Laser filamentation and self-focusing are phenomena familiar in laser fusion and can be seen clearly in Figs. 6 and 7. In Fig. 6, intense lasers ($V_{osc}/c \approx .5$) of width 20 c/ω_p incident from the left at first begin to filament into two narrower beams, then the strong radial gradient provides a pondermotive force which blows plasma out of the laser beam channels[19,20]. Pondermotive blowout is thought to be one of the major factors in the lack of accelerated electrons from a recent Los Alamos experiment. For very intense lasers, blowout can take place on a time scale as fast as the ion plasma period, necessitating the use of laser pulses shorter than this.

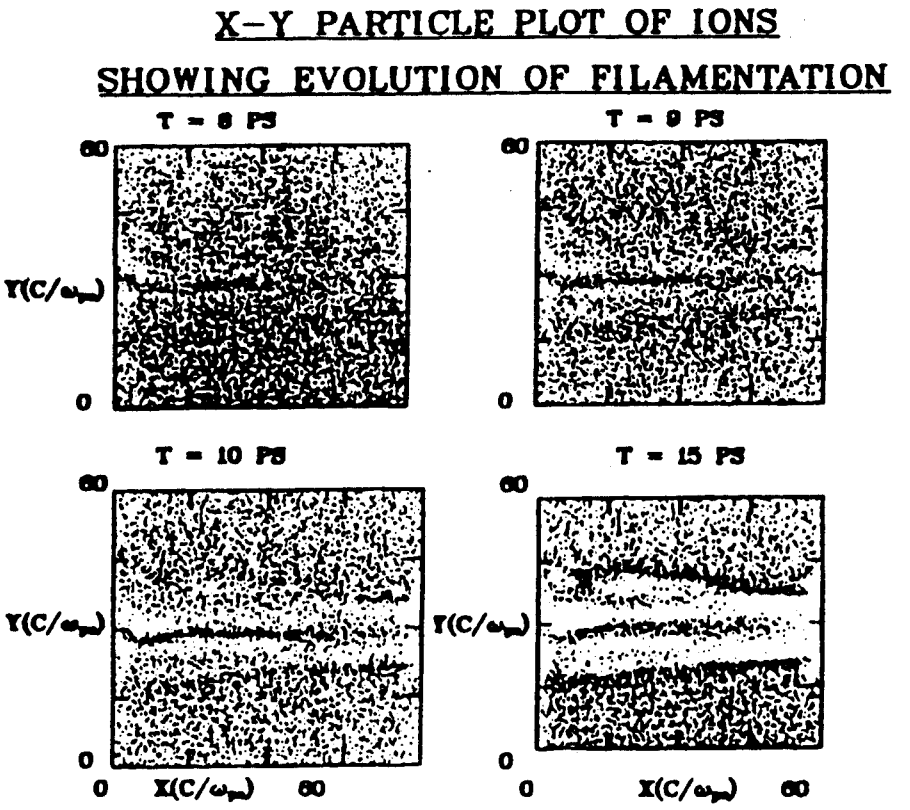

Fig. 6.

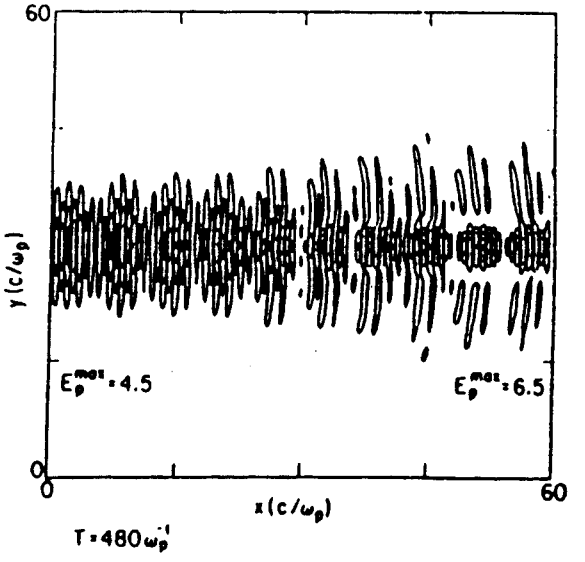

Fig. 7 2-D simulation contour plot of laser fields showing self-focusing (l to r) and increasing laser intenstiy on axis.

Laser self-focusing is a potentially beneficial phenomenon which may enable propagation of the lasers through the plasma over distances much longer than a Rayleigh length. In addition, as in Fig. 7, it may compensate for the depletion of pump intensity on axis (see Section II for a discussion of pump depletion). The mechanism for self-focusing can be understood quite simply by noting that the refractive index of a plasma is $n = (1-\omega_p^2/\omega^2)^{1/2}$. In a region of lower ω_p^2, the index of refraction is higher. Inside the plasma channel where the laser is, ω_p^2 $(=4\pi n_o e^2/m_e)$ is lower so the channel act like an optical fiber to confine the light. Inside the channel ω_p^2 is lower for two reasons. First, the plasma density can be slightly lower due to pondermotive blowout, and second, the oscillatory motion of the background electrons in the intense laser fields gives them a relativistic mass increase. The latter effect is probably more important because it may occur faster than an ion time scale. The time scale for self-focusing can be estimated from the inverse of the growth rate ν obtained by C. E. Max and J. Arons[21]:

$$\nu = \frac{\omega_p^2}{8\omega}\left(\frac{V_{osc}}{c}\right)^2 \tag{13}$$

The power threshold for self-focusing to overcome Rayleigh diffraction is approximately[22]

$$P \geq \frac{9}{2}\left(\frac{\omega}{\omega_p}\right)^2 \times 10^9 \text{ Watts} \tag{14}$$

Some question remains as to whether the final beam radius will asymptote or oscillate about a value of the order c/ω_p.

C. EXPERIMENTAL RESULTS

The first experimental verification of the theoretical and simulation models was performed recently at UCLA by C. Joshi, C. Clayton, C. Darrow, and D. Umstadter. A more detailed description of the experiment can be found in the paper by C. Joshi, et al., in these proceedings. The 9.6 and 10.6 micron lines of a CO_2 laser ($\alpha_{10.6} \approx .03$, $\alpha_{9.6} \approx .015$) were used to resonantly drive the beat wave in a $10^{17}/cm^{-3}$ density plasma. Modelling the lasers rise to be linear over 1 nsec, the model equations (8b) and (9b) predict a maximum normalized wave amplitude $\varepsilon = .08$ (or $E_L = 2.8$GeV/m) at a time of roughly 500 picoseconds.

In order to conclusively diagnose the beat wave, one needs to know the phase velocity and amplitude of the wave. The phase velocity was obtained by measuring the frequency shift of the light from a ruby laser which is scattered by the density modulations of the beat wave. A sample of the frequency spectrum of the scattered light is shown in Fig. 8. The frequency shift of the scattered light shows that the plasma wave frequency is centered at the beat

frequency of 9.6 and 10.6μ light. By varying the angle of the Thomson scattering, the k-spectrum of the plasma wave was obtained (Fig. 9). Figs. 8 and 9 together confirm that the phase velocity of the plasma wave was near c as predicted by Eq. (5).

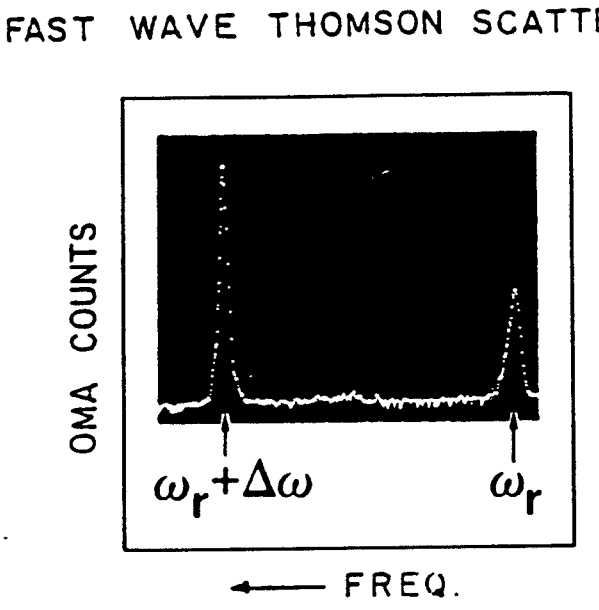

Fig. 8. Experimental small angle Thomson scattering indicating a plasma wave at the beat frequency ($\Delta\omega$) of the driving lasers (ω_r is the frequency of the diagnostic ruby laser).

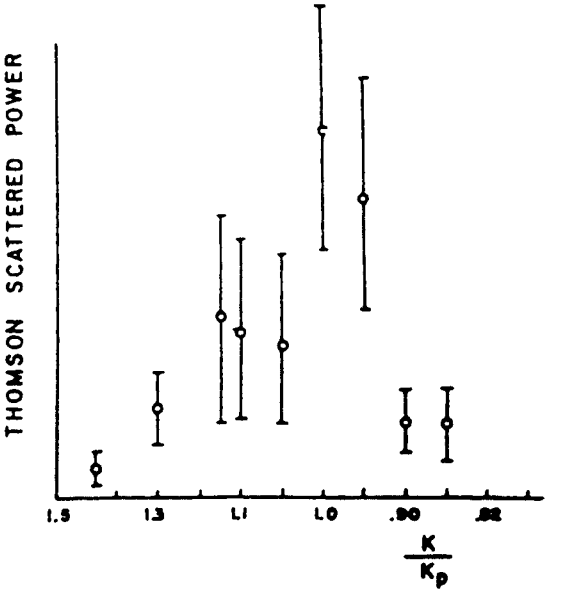

9. K-spectrum of the beat wave normalized to the theoretical beat wave wavenumber.

The time averaged plasma wave amplitude was obtained by measuring the intensity of the scattered light and calculating (assuming Bragg scattering from a moving grating) the corresponding n_1/n_0 (=ε) of the plasma wave. The resulting beat wave amplitude was n_1/n_0 = 1-3% or E_p = 330Mev/m -1GeV/m. This was the time-averaged field; the peak field may have been larger.

II ACCELERATION MECHANISMS

We now treat the acceleration of charged particles in the wave fields described in the previous section. Although it is not rigorous, we neglect the damping and distortion of the plasma waves by the accelerated particles. This is a fair approximation for moderate beams in which the number of beam particles per trapping potential is much less than the number of background plasma electrons in a plasma wavelength. Furthermore, we neglect the effect of the lasers on the accelerated particles. This is partially justified by the fact that in the beat wave frame, the laser electric field E_o is reduced by the Lorentz transformation to E_o/γ_{ph} and the magnetic field transforms away completely. The longitudinal plasma wave field on the other hand is invariant to transformations along the direction of particle acceleration, so we consider it alone in our treatment of charged particle motion. We rely on simulations to validate these approximations and to identify the important self-consistent effects.

A particle in the plasma cannot be picked up or trapped by the accelerating wave unless it exceeds a minimum velocity in the direction of the wave, much as a surfer must paddle to catch an ocean wave.

For this reason, the accelerated particles either must be injected externally or picked up out of the high energy tail of the background plasma distribution. Before proceeding to the beat wave and surfatron acceleration mechanisms, we first calculate the minimum velocity or injection threshold for particle trapping. This calculation will also provide an estimate of the maximum plasma wave amplitude ε before trapping of background particles becomes significant (catastrophically damping the wave).

A. INJECTION/TRAPPING THRESHOLD[23]

Consider a particle of velocity V and momentum γmV in the lab frame moving in the direction of a wave of high phase velocity, $V_{ph} \lesssim c$. Its energy γ' in the wave frame is given by the Lorentz transformation to be

$$\gamma' = \gamma_{ph}\ \gamma - \beta_{ph}\frac{P}{mc} \approx \gamma_{ph}\gamma(1 - \beta_{ph}\ V/c) \qquad (15)$$

where $\beta_{ph} = V_{ph}/c$ and $\gamma_{ph} = (1 - \beta^2_{ph})^{-1/2}$. A particle is just trapped by the wave when the wave' s potential (in the wave frame)

can overcome the particle's kinetic energy in the wave frame. That is, when

$$e\phi \geq (\gamma' - 1)mc^2 \tag{16}$$

the wave potential in the lab frame is simply

$$\phi = \phi'/\gamma_{ph} \tag{17}$$

since $E = k\phi$ is an invariant ($k'\phi' = k\phi$) and $k = \gamma_{ph}k'$. Combining Eqs. (15)--(17) gives the trapping potential

$$e\phi = mc^2\,[\gamma_{ph}\gamma(1 - \beta_{ph}V/c) - 1]/\gamma_{ph} \tag{18}$$

For $V = V_{ph}$, the minimum ϕ is zero as expected. Eq. (18) is valid for all particle and wave velocities. For $V/c \ll 1$ and $\gamma_{ph} \gg 1$, we find that

$$\phi/\phi_{cold} \approx 1 - V/c - 1/\gamma_{ph} \tag{19}$$

where ϕ_{cold} is the cold trapping threshold $\approx mc^2/e$ (from [18] with $V = 0$).

Interestingly, for electrons in the beat-wave example, cold trapping and cold wavebreaking (Eq. 2) are approximately the same threshold as can be verified from the above expression for ϕ_{cold} and $k = \omega_p/c$:

$$\underset{\substack{\text{cold}\\\text{trapping}}}{E} \approx k\,\phi_{cold} = kmc^2/e \approx mc\omega_p/e = \underset{\substack{\text{cold}\\\text{wavebreaking}}}{E}$$

Thus, to the extent that $|E| \approx |k\phi|$ for the plasma wave, $\phi/\phi_{cold} \approx \varepsilon \approx E/E_{max}$ (for $\gamma_{ph} \gg 1$). We comment that for ions, the cold trapping threshold would be larger than the cold wavebreaking threshold by the ion to electron mass ratio. Thus, trapping of ions will be much more difficult and will require the ions' velocity to be essentially V_{ph}.

We expect to trap few background particles if (19) is satisfied for V = a few (e.g., 3) times the thermal velocity (V_t). Thus, one should take ε less than $1 - 3V_t/c$ ($V_t \ll c$) to assure a minimum of background plasma trapping.

Expression (18) may be used to estimate what injection velocity or injection energy is required for injected particles to be picked up by a wave of given amplitude. Inverting (18) and solving for the injection energy ($\gamma - 1$) in terms of $\phi/\phi_{cold} \equiv e\phi/mc^2 \approx \varepsilon$ yields

$$\gamma - 1 \approx \gamma_{ph}^2\,\{\varepsilon + 1/\gamma_{ph} - \beta_{ph}\,|(\varepsilon + 2/\gamma_{ph})\varepsilon|^{1/2}\} - 1 \tag{20}$$

Thus, for example if $\phi/\phi_{cold} = .1$ and $\gamma_{ph} = 10$, then the injection energy must be about 900 keV.

The injection energies versus normalized wave amplitude ε from Eqs. (18) or (20) are plotted for several values of γ_{ph} in Fig. 10.

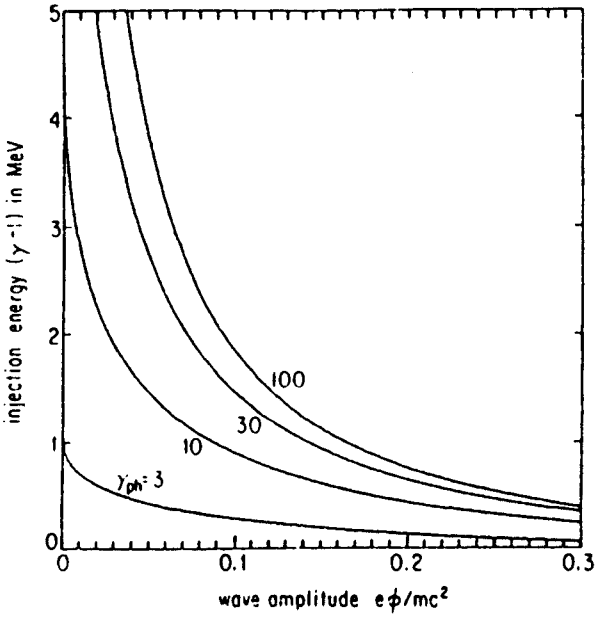

Fig. 10 Injection energy thresholds vs. normalized wave amplitude for various wave phase velocities (from Eq. 20).

B. SIMPLE BEAT WAVE ACCELERATION

In the original beat wave accelerator (BWA) concept, a particle accelerates by simply riding from the top to the bottom of the potential well of a plasma wave (i.e., a half of the plasma wavelength λ_p). Since the plasma wave moves at $V_{ph} = c\,(1 - \omega_p^2/\omega^2)^{1/2} \approx c(1 - \omega_p^2/2\omega^2)$ [see Eq. (5)] and the particle moves at nearly c,[24] the particle outruns the wave (reaches the bottom of the potential well) in a distance

$$\ell = (\lambda_p/2)\, c/(c - V_{ph}) \approx (\omega^2/\omega_p^2)\lambda_p \qquad (21)$$

The maximum energy gain of the particles is of order $eE_p \cdot \ell$ or

$$W_{max} = 2\varepsilon \frac{\omega^2}{\omega_p^2}\, mc^2 \qquad (22)$$

where we have substituted $\lambda_p = 2\pi c/\omega_p$, ε is the plasma wave amplitude normalized to wavebreaking and we have taken the average value of E_p to be its amplitude over π in order to give a result consistent with other derivations[24].

The energy gain[22] can be quite large. For example, for 1μ laser radiation incident on a $10^{17}/cm^{-3}$ plasma, $\omega/\omega_p = 100$ and the maximum energy gain is 20GeV in a distance less than a meter (for ε near 1).

We comment that the actual region of the plasma wave useable for acceleration is likely to be less than $\lambda_p/2$. Radial fields due to the finite width of the plasma wave are defocusing to particles over part (5/16) of the accelerating portion of the plasma wave[25]. If the width of the plasma wave is given by the laser beam width and this in turn self-focuses to a few times c/ω_p as discussed in Section I, then the radial fields will be quite large and it will be necessary to avoid the regions of defocusing.

1-D simulations performed prior to the first laser accelerator workshop verified electron acceleration consistent with Eq. (22). Recent 2-D simulations[18] have substantiated the 1-D results and added information about the transverse particle dynamics. The phase space plots of Fig. 11 illustrate both electron acceleration in the plasma wave troughs and the focusing of the accelerated particles in the transverse direction. The peak γ of particles in Fig. 11 is around 25, consistent with Eq. (22) and the simulation parameters ($\epsilon \sim .5$, $\omega_1 = 4\omega_p$, $\omega_2 = 5\omega_p$).

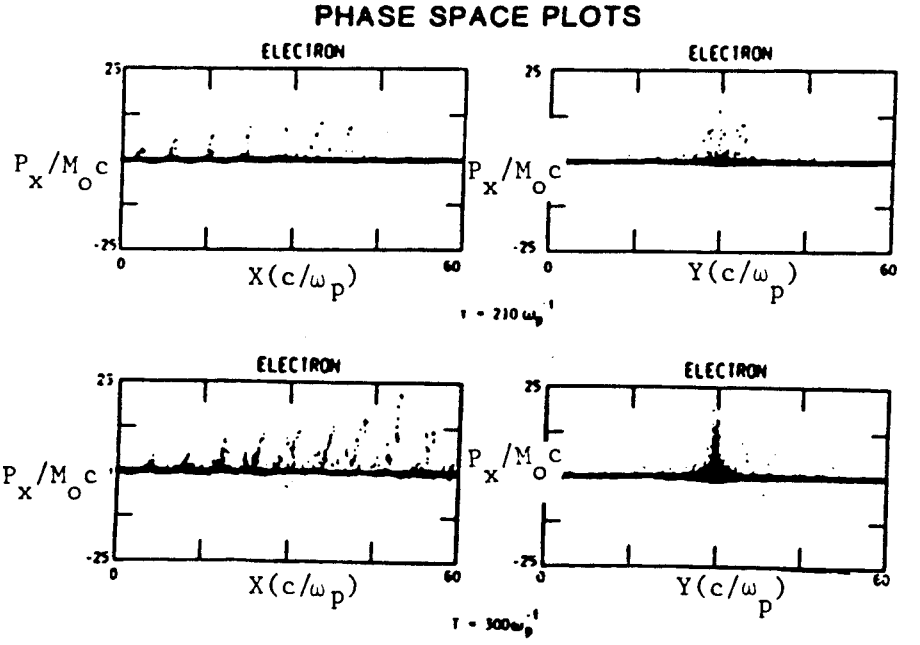

Fig. 11 2-D simulations showing acceleration in plasma wave troughs (left) and particle focusing (right) at two different times.

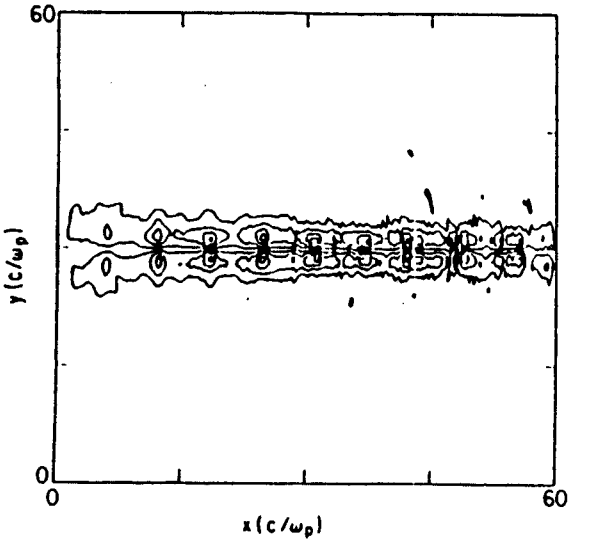

Fig. 12 Contour plot of azimuthal magnetic field (B_Z) in a 2-D simulation. The field near the bunches of accelerated electrons corresponds to Megagauss for CO_2 laser parameters.

Particle focusing is important to the emittance quality of the accelerated beam. We believe that the particle focusing in Fig. 11 is caused by the self-generated magnetic fields of the accelerated electron bunches. A contour plot of the azimuthal magnetic field is shown in Fig. 12. The magnetic field concentrated near each bunch would correspond roughly to 2 megagauss for CO_2 laser parameters. Although this field cannot confine a beam in vacuum because the space charge repulsion of the beam electrons cause them to diverge, in a plasma the space charge of the beam is partly neutralized by the background plasma[26]. Thus the $\vec{V} \times \vec{B}_\theta$ force on beam particles off axis pinches them toward the center.

C. THE SURFATRON ACCELERATION MECHANISM

Expression (22) for the maximum energy gain of the BWA suggests that the lower is ω_p^2 (i.e., the lower the plasma density), the higher is the final energy that can be obtained. Then why not eliminate the plasma so that the maximum energy can become infinite? The answer of course is contained in Eq. (2) which shows that the acceleration gradient ($\Delta W/\Delta x$) goes to zero. These two equations illustrate the beat wave dilemma:

$$W_{MAX} \sim \frac{1}{n_o}$$

$$\Delta W/\Delta x \sim \sqrt{n_o}$$

The higher the final energy required of the beat wave accelerator, the slower the acceleration gradient. For example, the maximum gradient possible in a plasma of density $10^{18}cm^{-3}$ is an impressive 1GeV/cm, but the effective acceleration length (for CO_2 parameters) is only .01 cm. If the accelerator is allowed to be any longer than this, the particle will pass the bottom of the plasma wave potential well and begin giving energy back to the plasma wave as it proceeds up the next potential hill.

The surfatron[27] is proposed as a mechanism to overcome this limitation of the BWA by phase locking the particles in the plasma wave, thereby allowing them to gain energy for as far as the plasma wave can be maintained. The basic idea, illustrated in Fig. 13, is to impose a DC magnetic field (B_z) perpendicular to the beat wave. The $-e\vec{V}_{ph} \times \vec{B}/c$ force on a trapped particle deflects the particle across the wave fronts similar to the way a surfer cuts across the face of an ocean wave. Once the particle acquires y-velocity the $-e\vec{V}_y \times \vec{B}/c$ force presses the particle up against the side of the wave where it remains phase locked.

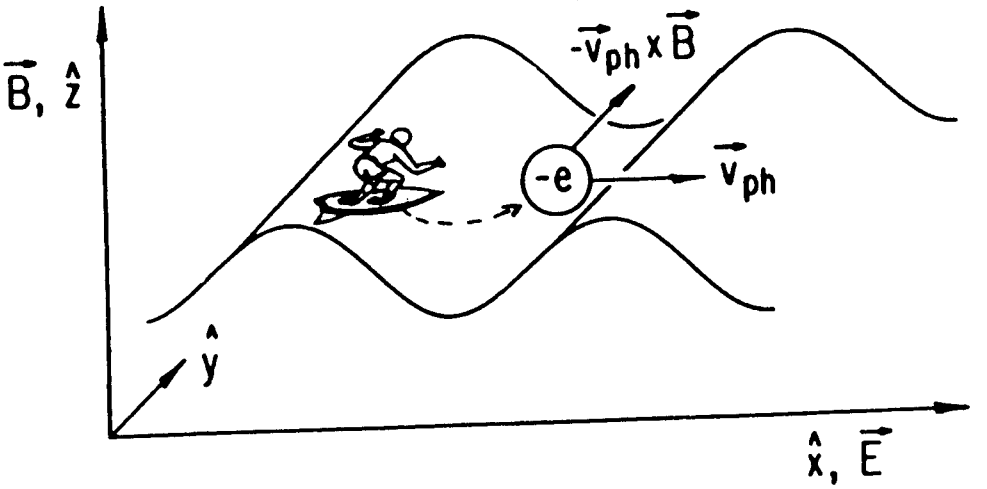

Fig. 13 A DC magnetic field deflects particles across the waves in the surfatron, preventing them from outrunning the waves.

In the wave frame (Fig. 14), the accelerated particle comes to a phase stable point in the potential well where the electric force ($E_p \sin k' x_1'$, primes denote wave frame quantities) of the plasma wave balances the magnetic force ($V_y' B_z'/C \approx \gamma_{ph} B_z$) due to motion across the wave.

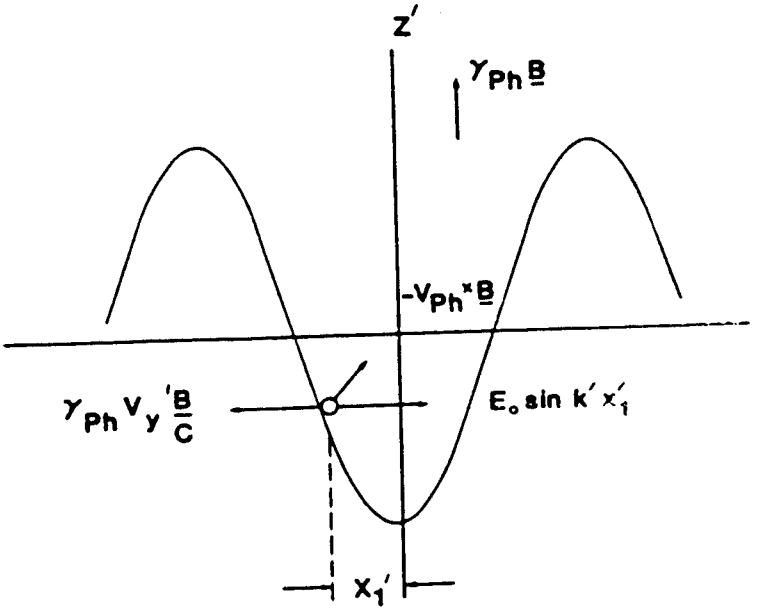

Fig. 14 In the wave frame, a surfatron particle comes to equilibrium against the side of the potential well.

Since $\sin k'x_1' \leq 1$, we must have

$$E_p > \gamma_{ph} B_z \tag{23}$$

in order to have a phase stable point. Too large a magnetic field will cause the particle to detrap and exhibit cyclotron motion.

If the wave phase velocity is near c, the particle travels a nearly linear trajectory at a small angle (θ) to the direction of the plasma wave. This can easily be seen from the fact that for a trapped relativistic particle

$$V_x \approx V_{ph}, \quad V_x^2 + V_y^2 \approx c^2 \tag{24}$$

Thus

$$\tan\theta = V_y/V_x \approx 1/\gamma_{ph}. \tag{25}$$

That the trajectory is linear assures that the radiation from surfatron acceleration is not large. Although it was first thought that radiation is less from surfatron acceleration than linear acceleration, it has been pointed out[28] that for the same $d\gamma/dt$, radiation from a linac and surfatron are the same.

The rate of energy gain for a surfatron particle is most easily obtained from the $\hat{y}$ equation of motion in the lab frame:

$$\frac{d}{dt}(\gamma V_y) = \omega_c V_x \tag{26}$$

where $\omega_c = eB_z/mc$, the non-relativistic cyclotron frequency. Substituting for V_x and V_y from (24) and integrating once gives the energy gain versus time or distance.

$$\gamma = \gamma_{ph}\,(V_{ph}/c)\,\omega_c t = \gamma_{ph}\,\omega_c x/c \tag{27}$$

Numerical solutions of surfatron motion in a sinusoidal plane wave electric field and uniform magnetic field are shown in Fig. 15b. The particles' energy increases linearly according to (27), and the fractional energy spread $\Delta\gamma/\gamma$ of two particles decreases as they both approach the same phase stable point. The BWA particles of Fig. 15a on the other hand spread in energy as they asymptote to the BWA limit (22). In Fig. 16, the phase space plot from a 1-D simulation shows surfatron motion in agreement with Eq. (26).

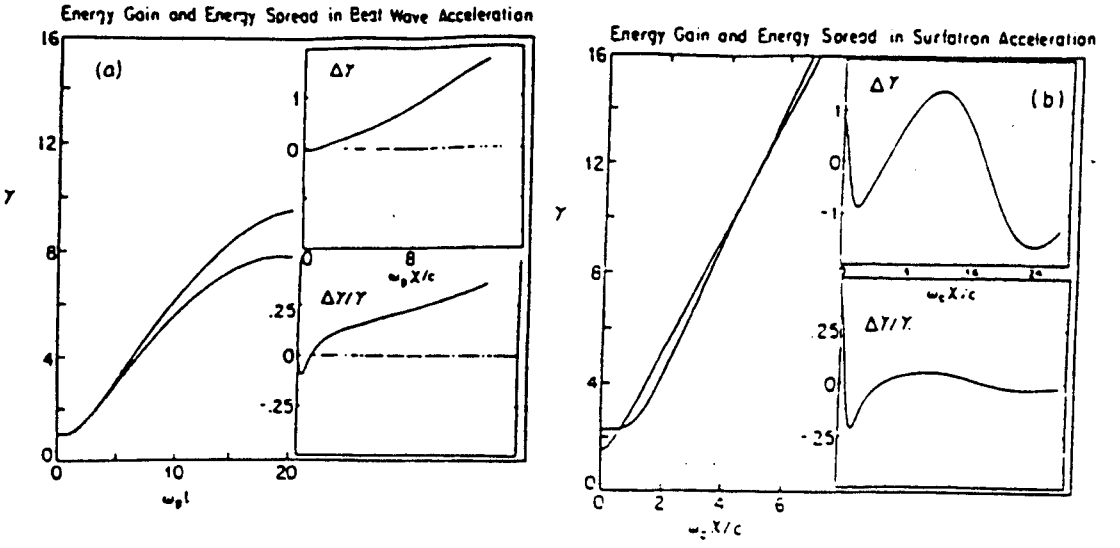

Fig. 15 Energy gain and spread for (a) two BWA particles and (b) two surfatron particles.

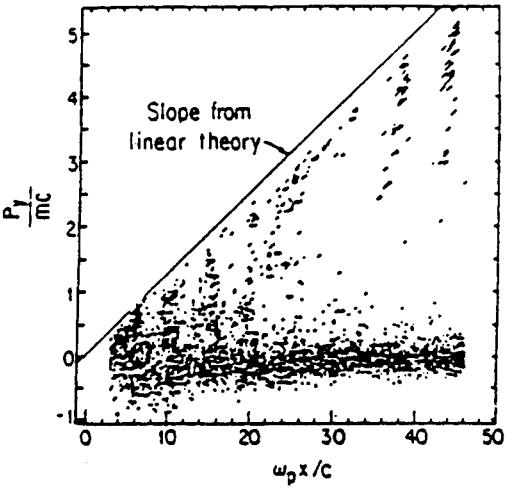

Fig. 16 Electron momentum across the wave P_y vs. distance x in a 1-D surfatron simulation.

The accelerating gradient, angle θ and trapping inequality for the surfatron can be summarized by the following formulae, valid for either electrons or protons:

$$\frac{\Delta W}{\Delta x} = \sqrt{n_{16}}\ \left(\frac{B_{kG}}{n_{16}\lambda\mu}\right)\ .1\ \text{GeV/cm} \qquad (28)$$

$$\theta \approx \lambda_\mu \sqrt{n_{16}}/300 \tag{29}$$

$$B_{kG}/n_{16}\lambda_\mu < \varepsilon = E_p/E_{wavebreak} \tag{30}$$

where n_{16} denotes the plasma density in units of $10^{16}cm^{-3}$, B_{kG} is B_z in kilogauss, λ_μ is laser wavelength in microns and we have substituted $\gamma_{ph} = \omega/\omega_p$ from Eq. (5) and the definition of γ_{ph}. The accelerating gradient is roughly that of the BWA if B_z is chosen to make the trapping inequality (30) nearly an equality.

As an example, let us compare rough design parameters (Table I) for a 1TeV single stage BWA and surfatron accelerator using 1 micron laser light and assuming $\varepsilon \approx .5$. For the surfatron, we take $n = 10^{18}cm^{-3}$ and B = 50kG; for the BWA the density will have to be lower (from Eq. 22).

TABLE I COMPARISON OF DEVICE SIZES TO REACH 1 TeV

Device	Energy	Length	Width
Conventional	1 TeV	10-50 km	--
BWA	1 TeV	600 m	--
Surfatron	1 TeV	20 m	.6 m
Surfatron w/ optical mixing	1 TeV	20 m	.1 m

OPTICAL MIXING

As the above table indicates, a pure surfatron accelerator requires a fairly wide wavefront (.6m in this example). However, the particle trajectory is nearly linear, so much of the wave energy is wasted (see Fig. 17). C. Joshi and F.F. Chen have suggested that by optically mixing the beating lasers at a slight angle the energy can be confined along the particle path while preserving the proper wavefront geometry[29,30]. The electrons follow the path of the low frequency laser (ω_1, $\vec{k}_1$), while the high frequency laser (ω_0, $\vec{k}_0$) propagates at a small angle ϕ to the electrons.

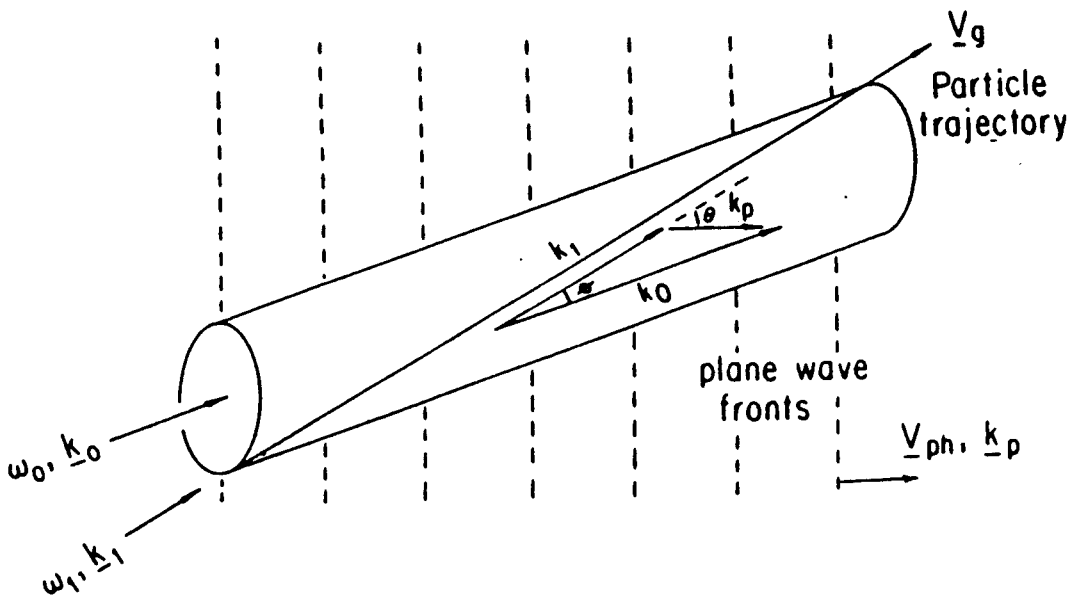

Fig. 17 By optically mixing the two lasers at small angle ϕ, the surfatron wave geometry can be created (wave fronts at angle θ to particle trajectory) without the need for a wide wavefront.

Optical mixing has two advantages. First, the wave width and laser energy requirements are greatly reduced. Second, the lasers are no longer co-linear with the particle beam, thereby allowing much easier staging.

From Fig. 17 and the law of sines

$$\sin\phi = k_p/k_o \sin\theta << \sin\theta \tag{31}$$

so that the width of surfatron of length L need only be $L\sin\phi$ rather than $L\sin\theta$. From the fluid model of Section I, we expect the beat wave growth to be proportional to the product $E_o E_1$ of the two laser fields. Thus, we can let the lower frequency narrower laser E_1 be the more intense beam and reduce the intensity of the wider beam, while maintaining the beat wave amplitude. This lowers the energy requirement by more than just the width ratio of the devices.

The small mixing angle ϕ can be calculated from Fig. 17, Eq. (31) and the combination of the law of cosines, the dispersion relations ($\omega_i^2 = \omega_p^2 + c^2 k_i^2$, $i = 0,1$), and the condition that the component of V_{ph} along k_1 ($\omega_p/k_p \cos\theta$) be c. The result is[30]

$$\phi \approx \left(\frac{\omega_p}{\omega_o}\right)^{3/2}$$

The generation of a small angle optically mixed beat wave has been supported by the 2-D simulations shown in Fig. 18. The first

figure shows the contour plot of the beating between a narrow laser on axis and a wide laser at a small angle. The second figure shows that the corresponding plasma wave fronts are confined along the axis but tilted at the desired angle.

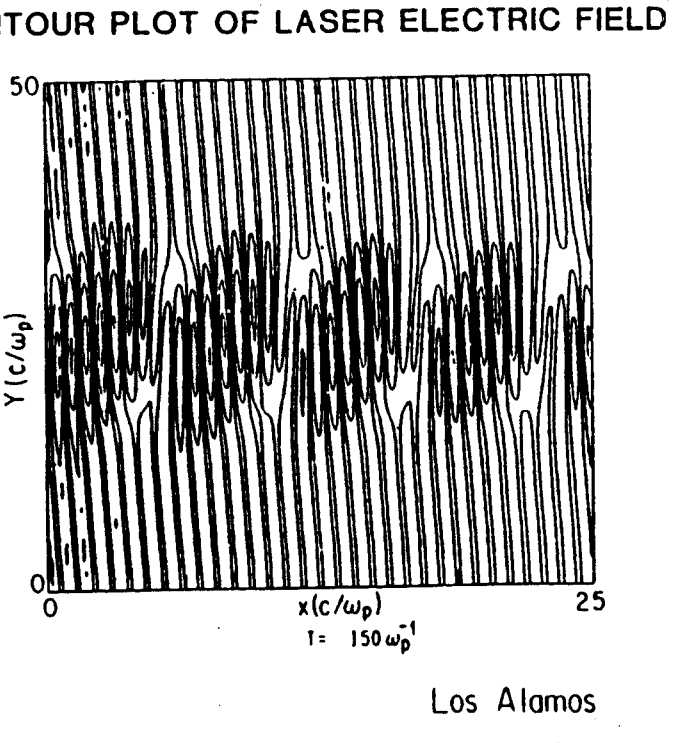

Fig. 18 2-d simulation contour plots of (a) the small angle optically mixed laser fields and (b) the resulting plasma waves.

Since the particles in optical mixing move at c nearly parallel to the light pulse at V_g, the particles will eventually overtake the light pulse. If the particles are injected several (N) wavelengths behind the pusle (see Fig. 2), the distance for this overtaking to occur will be $\ell = N\lambda_p c/(c - V_g) \approx 2N\lambda_p \omega^2/\omega_p^2$. This is much longer than the limiting distance for the BWA (Eq. 21). As we shall see in the next section, pump depletion limits the length of acceleration before this velocity mismatch ever becomes a problem.

PUMP DEPLETION

Unfortunately, simulations of surfatron acceleration failed to show energy more than about 30% higher than corresponding BWA runs. Energy gain in the surfatron scheme is not limited by particle dynamics; it is limited instead by wave dynamics. That is, the laser pulse/plasma wake package of Fig. 2 cannot be propagated indefinitely through the plasma. The laser pulse is continually feeding energy into plasma waves. Since the plasma wave energy convects at the plasma wave group velocity ($\sqrt{3}\, V_{th}^2/V_{ph}$) which is effectively zero, all of the plasma wave energy is left behind. When the energy left in plasma waves becomes comparable to the energy originally in the laser pulse, the laser pulse will have become completely depleted and no more plasma waves can be produced. We can estimate this pump depletion length L_d from the simple energy balance argument that the energy density of the plasma waves times L_d must be less than the energy per unit area in the laser pulse:

$$\frac{E_p^2}{8\pi} \cdot L_d \leq 2 \int_0^\tau \frac{E_o^2(t)\, dt}{8\pi}$$

where we assume both lasers to have amplitude E_o, $\ell/c = \tau$ the length of the laser pulse, E_p is the amplitude of the plasma waves and we have assumed equal cross-sectional areas for laser and plasma waves. Adopting our previous normalizations, we have

$$L_d \leq \frac{\omega_o^2}{\omega_p^2} \frac{\int^\tau a_o^2\, dt}{\varepsilon^2}$$

If we assume the maximum effective length τ of our laser pulse to be determined by relativistic detuning (Eqs. 8b and 9b) and substitute one factor of ε from Eq. (8b), we find that

$$L_d \leq \frac{\omega_o^2}{\omega_p^2} \frac{c}{\omega_p} \frac{4}{\varepsilon} \tag{32}$$

independent of pulse shape. Since L_d is the distance that the laser can propagate into the plasma before becoming depleted, it is also the maximum acceleration length for the surfatron. Surprisingly, the maximum surfatron particle energy is independent of laser

intensity since the energy gain is proportional to εL_d. In fact, for α greater than about .4, the plasma wave can reach wavebreaking before relativistic detuning occurs, further shortening τ and L_d.

Comparison to Eq. (21) for the dephasing length ℓ of particles in the BWA shows that L_d exceeds ℓ by only the factor $1/\varepsilon$ (neglecting a numerical factor which is approximately 1). We expect the energy gain in the surfatron and BWA to scale as

$$\frac{\Delta\gamma \text{ (surf.)}}{\Delta\gamma \text{ (BWA)}} \approx 1/\varepsilon.$$

THis is somewhat optimistic since not all of the laser pulse can be effectively converted to plasma waves. On the other hand, if the laser beats could be detuned to avoid the relativistic detuning discussed in Section I, then the effective laser pulse length τ, and consequently L_d, could be increased. Presumably τ would then be limited to about $2\pi/\omega_{pi}$ (or a few times this), the time for competing ion instabilities to degrade the plasma wave.

A final problem we have observed in surfatron simulations is the more rapid onset of turbulence in the plasma wave train. The predicted surfatron acceleration is observed for particles in the first few plasma troughs. The degradation of the later troughs seems to coincide with the development of the large self-induced magnetic fields (see section I-B) of the accelerated particles. It is not clear why the plasma wave dynamics are so different for the surfatron than the BWA since the applied DC field is relatively small ($\omega_c/\omega_p < \varepsilon/\gamma_{ph} \ll 1$ by the trapping inequality [30]).

III NEW IDEAS FOR PLASMA ACCELERATORS

A. RIPPLED PLASMA OR PLASMA GRATING ACCELERATOR

It may be possible to overcome the pump depletion problem of the previous section by employing a non-colinear laser geometry to excite the plasma waves. Fig. 19 illustrates a mechanism for a side-injected accelerator in which a single incident laser is polarized along the direction of a static density ripple in the plasma[31]

$$n(x) = n_o + \delta n \sin k_r x$$

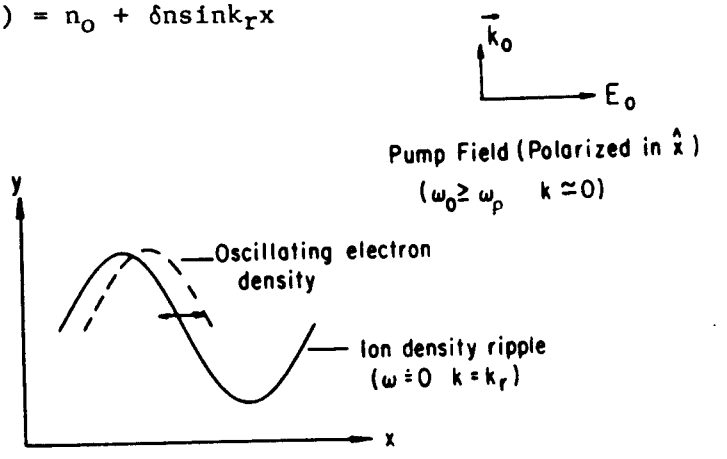

Fig. 19 A single laser incident from the side oscillates the electrons of a density rippled plasma to drive a longitudinal plasma wave in the direction of laser polarization.

Such a ripple might be produced by an ion acoustic wave or by ionizing a grating.

The laser field wiggles the electrons in the ripple by an amount

$$\delta x = (eE_o/m\omega_o^2)\cos\omega_o t$$

while the ions are too massive to respond. This produces a longitudinal electric field distrubance given by Poisson's equation:

$$\frac{\partial E_p}{\partial x} = 4\pi e\delta n_e = 4\pi e\frac{\partial n}{\partial x}\delta x \approx \frac{\omega_p^2}{\omega_o^2}E_o\frac{\delta n}{n_o}k_r\cos k_r x\cos\omega_o t$$

The right hand side represents a driver for the plasma wave which is bilinear in $\delta n/n_o$ and E_o and is analogous to the beat wave ponderomotive force which is bilinear in E_1 and E_2 of the two lasers. In fact, for $\omega_o \gtrsim \omega_p$, the initial plasma wave growth is

$$\varepsilon(t) = \frac{\alpha_o(\delta n/n_o)}{4}\omega_p t \qquad \varepsilon \equiv eE_p/m\omega_p c,\ \delta n/n_o \ll 1$$

which is identical to Eq. (8) for the beat wave if $\delta n/n_o$ replaces α of the second laser. Since the interaction is only quasi-resonant ($\omega_o > \omega_p$ to allow the laser to propagate into the plasma), the plasma wave saturation is determined by the detuning of the laser and plasma frequencies:

$$\varepsilon_{max} \approx \frac{\alpha_o\delta n/n_o}{2(\omega-\omega_p)} \qquad (\text{for } \varepsilon_{max} < 1)$$

The phase velocity of the plasma wave is determined by the coupling between the laser (ω_o, $\vec{k}_o$) and the ripple or acoustic wave (ω_r, $\vec{k}_r$). By choosing ω_o near ω_p, the dispersion relation for the laser $\omega_o^2 = \omega_p^2 + k_o^2c^2$ indicates that k_o will be small. Thus

$$V_{ph} = \frac{\omega_p}{k_p} = \frac{\omega_o + \omega_r}{|\vec{k}_o \pm \vec{k}_r|} \approx \frac{\omega_o}{k_r}$$

The phase velocity of the plasma wave can be controlled by varying the ripple wavenumber. The phase velocity might be increased along the accelerator to keep up with the accelerated particles or, alternatively, the particles might be surfed. Preliminary 1-D simulations of surfatron motion with an applied magnetic field show acceleration well past the unmagnetized limit [obtained from Eq. (22) with the replacement $\omega^2/\omega_p^2 \to \gamma_{ph}^2 = (1 - \omega_p^2/k_r^2c^2)^{-1}$] without the pump depletion problem. Figure 20 shows the background ripple and accelerated particles in the corresponding plasma waves of a 1-D simulation.

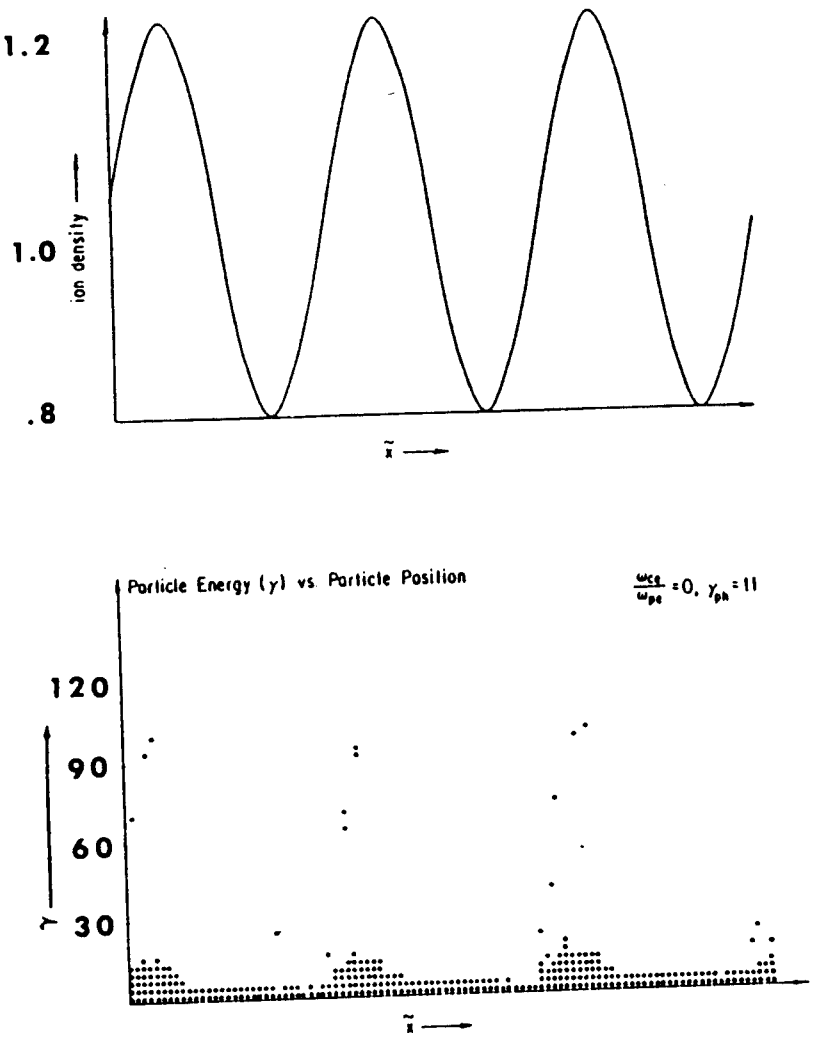

Fig. 20 1-D simulations showing (a) the initial density ripple and (b) the electron energy gained in the resulting plasma wave.

Figure 21 shows a 2-D simulation performed by W. Mori, K. Lee, D. Forslund, and J. Kindel. In this case, an intense laser is incident on a periodic array of neutral droplets rather than a density ripple. The original intention was to demonstrate near field acceleration in the normal modes of the droplet structure. Instead, the droplets were quickly ionized, forming a rippled plasma with density peaks centered at each ball. Preferred acceleration was then observed in the direction of laser polarization as in the present mechanism. At high laser intensity many schemes may unintentionally become plasma schemes. In this case, the plasma properties may actually be used to advantage.

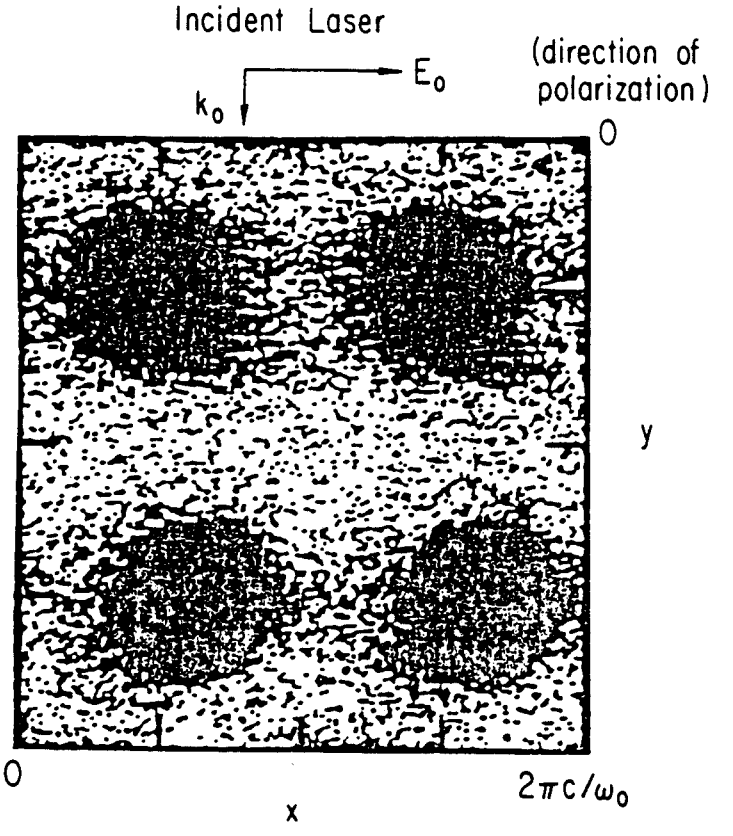

Fig. 21 2-d simulation of lasers incident on neutral droplets showing rapid formation of a (density-rippled) plasma or plasma grating.

B. CONVERGING PLASMA WAVES

Another scheme which employs a non-colinear geometry is illustrated in Fig. 22[32]. Two sets of plasma waves converge at a slight angle and particles are accelerated down the axis of symmetry between them in the superimposed fields. The phase velocity down the axis is higher than the phase velocity of the individual plasma waves (see Fig. 22b) and can be controlled by the angle θ at which the waves converge. This avoids the phase slip problem of the BWA, and the non-colinear injection facilitates resupplying the driving energy. Energy gain per stage will exceed that of the BWA if

$\omega_p a/c > \omega/\omega_p$

where a is wave width.

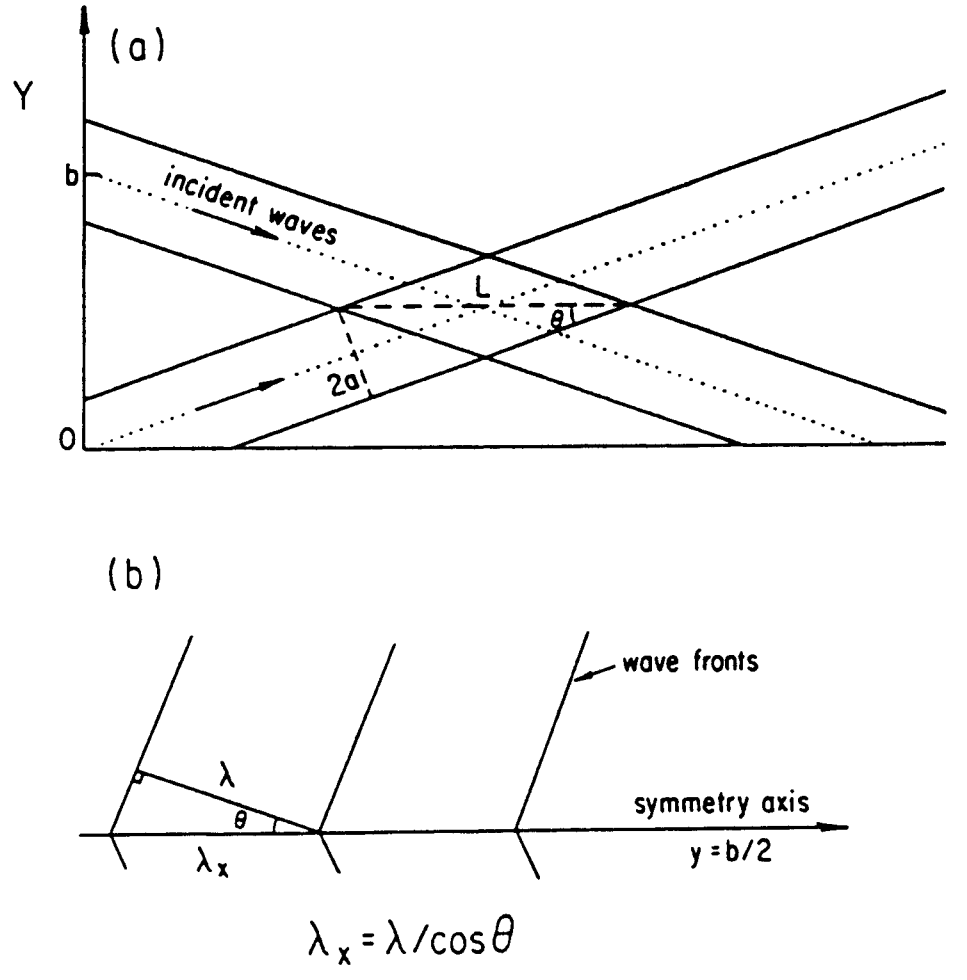

Fig. 22 A converging wave geometry (a) facilitates re-supplying the driving energy and (b) enables a higher phase velocity down the symmetry axis.

Figure 23 shows numerical solutions of (a) particle trajectories and (b) their corresponding energy gain in two sets of converging logitudinal plane wave electric fields of gaussian width a. The particles gain energy in each of the interaction regions and are either focused or defocused depending on their phase. If the focusing properties can be taken advantage of, they might offset the factor of two (or more) waste of plasma wave energy in regions where particles are not being accelerated.

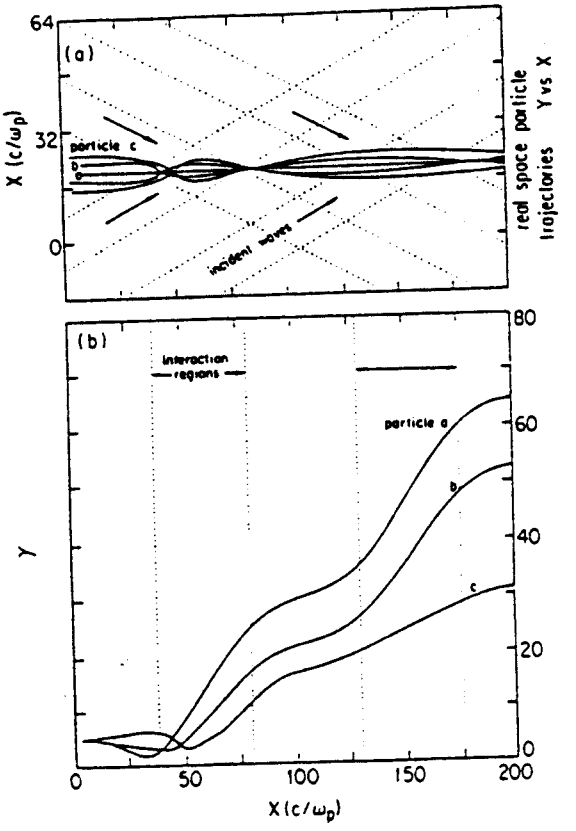

Fig. 23 Numerical solutions of (a) particle trajectories and (b) energy gain in the field geometry of Fig. 22.

In order to create the desired geometry, two pairs of beating lasers might be used. In this case, we must have $\omega_1 - \omega_2 \cong \omega_p \cong \omega_3 - \omega_4$, but $\omega_1 - \omega_4 \neq \omega_p$ to avoid unwanted couplings in the interaction region. Another way to create the waves might be to use the non-laser plasma wakefield scheme.

C. THE PLASMA WAKEFIELD ACCELERATOR

The Plasma Wakefield Accelerator[9] is a non-laser accelerator scheme which utilizes the electron bunches of a conventional linac as the free energy source to drive the plasma waves. If a later arriving, less dense, bunch of electrons is properly phased, it can ride the plasma waves or wakes of the earlier bunches and be accelerated.

The mechanism for exciting the plasma waves is similar to the plasma two stream instability except that the electron beam is made up of discrete bunches rather than a continuous stream. It is hoped that by controlling the spacing between bunches that the plasma wavelength and hence phase velocity can be controlled. The phase

velocity of the pure two stream instability on the other hand is always slightly less than the stream[33] velocity with deleterious consequences for maximum energy gain.

The electric field gradients (i.e., wakefield amplitudes) possible in this scheme scale as the Coulomb Field of a driving bunch at a distance of a plasma wavelength[9]:

$$eE \sim \frac{Ne^2}{(c/\omega_p)^2}$$

where N = the number of electrons per bunch. For example, a bunch of $N = 5 \times 10^{10}$ electrons can produce a Wakefield which is near the wavebreaking amplitude in a $10^{15} cm^{-3}$ density plasma. However, the bunch length must be less than $c/\omega_p \approx .2$ mm.

In a colinear geometry, the energy transferred to a driven electron is limited by the wakefield theorem of Ruth, et al.[9], to be less than two times the energy per driving electron. To overcome this limit may require a non-colinear scheme such as that suggested in the preceeding section. Since this workshop, the use of a non-symmetric driving bunch has been proposed[34]. This overcomes the wakefield theorem and enables bunch lengths longer than c/ω_p.

IV SUMMARY

A great deal of progress has been made on plasma accelerators since the first workshop in 1982. The beat wave accelerator is becoming well developed. The growth and saturation of the beat waves is now predictable from a modified fluid model which includes the laser rise time and frequency detuning. This model gives excellent quantitative agreement with one and two dimensional computer simulations. The extension of the simulation models to 2-D has guided our understanding of effects such as laser and particle self-focusing and competing instabilities.

The theoretical and computational progress has now been complimented by the recent UCLA experiment. The UCLA results demonstrated the first conclusive experimental evidence of a beat excited fast plasma wave with an electric field on the order of 1GeV/m.

The surfatron has been proposed as a means of overcoming the energy limitation of the beat wave accelerator. A number of problems and solutions associated with the surfatron phase locking scheme have been addressed. Small angle optical mixing appears promising for reducing the width requirement of the accelerating wave. Laser detuning or "chirping" may be necessary to increase the pump depletion length and enable the surfatron to exceed the BWA in energy. Finally, if problems associated with the self-generated magnetic fields of the accelerated beam can be overcome, the surfatron enables acceleration of higher quality beams ($\Delta\gamma/\gamma \to 0$) of electrons or protons.

New ideas for acceleration in a plasma medium are constantly being explored, each with its own advantages. The plasma grating scheme described here is attractive because (a) the laser energy is injected from the side, thereby avoiding pump depletion problems, (b) only a single laser frequency is required and (c) the plasma wave phase velocity can be controlled with the density ripple or ionized grating separation. The plasma wakefield accelerator takes advantage of the efficiency and high power that are available from existing accelerator technology. Both schemes are at an early stage of development.

With the understanding gained from the simulation models and the UCLA experiment, the prospects are good for a successful proof-of-principle beat wave experiment in the next three years, contingent upon funding. Equations (8b) and (9b) provide a design guide for the laser and plasma waves. Equation (20) predicts the required injection energy and Eq. (22) gives the expected final energy. Based on these equations, table II provides a reasonable reference design for a near term experiment.

Table II LASER AND PLASMA PARAMETERS FOR A BWA EXPERIMENT

CO_2 Laser	10.6 μm, 10.3 μm
Pressure	5 atmospheres
Pulse length	30-50 ps
Intensity	5×10^{13} W/cm^2 (10J)
Focal Spot Radius	400 μm
Rayleigh Length	10 cm
Plasma Density	10^{16} cm^{-3}
Acceleration Gradient	~ 1 GeV/m
Acceleration Length	~ 10 cm
Initial Beam Energy	~ 5 MeV
Final Beam Energy	~ 100 MeV

Work continues toward realizing the high gradients, immunity from breakdown, and focusing properties that plasma accelerators offer.

ACKNOWLEDGMENT

We are grateful to Drs. J. Kindel, D. Forslund, and K. Lee for their collaboration on most of the simulations; to Drs. P. Chen and R. W. Huff for sharing their plasma wakefield work; to D. Sultana for her rippled plasma simulation; and to Dr. W. Horton for helpful comments.

Thanks to J. Rose and J. Payne for help in preparing the final manuscript.

Work supported by US DOE contract DE-AT03-83ER 40120, NSF grant ECS 83-10972, NSF grant PHY 83-04641, and Lawrence Livermore Laboratory's University Research Program.

REFERENCES

1. D. Lowenthal, see these proceedings.

2. J.D. Jackson, Classical Electrodynamics, 2nd ed., Section 6.8 (John Wiley & Sons, New York, 1975).

3. The radiation or pondermotive force on a single electron at rest in a light wave $\vec{E} = \hat{y}E_y\sin(kx-\omega t)$ is $F_p' = k'e^2E_y'^2/2\omega'^2$ (see Eq. 6 of the text), where primes denote quantities in the particle's rest frame. If the particle were moving relativistically along $\hat{x}$, then $E_y' = \gamma(E_y-\beta B_z) \approx E_y/2\gamma$, $\omega' \sim \omega/2\gamma$ $k' \sim k/2\gamma$, $Fp = \frac{dp}{dt} = 2\frac{dp'}{dt'} = 2Fp'$, so that $Fp = ke^2E_y^2/2\gamma\omega^2 \propto 1/\gamma$. This derivation was suggested to me by G. Schmidt; a Hamiltonian-Jacobi treatment is in Landau and Lifshitz, Classical Theory of Fields, Section 47 (Addison-Wesley, Reading, Mass., 1971), 3rd ed.

4. An exact non-linear solution to the relativistic cold fluid equations [Akhiezer and Polovin, Sol. Phys., JETP 3, 696 (1956)] shows that the maximum electric field of a highly relativistic wave can exceed this value. Their result is $eE \approx m\omega_p c(\gamma_{ph}-1)^{1/2}$. Additionally, a waterbag model of a warm plasma can be used to estimate the thermal corrections (See Ref. 23) with the result that $e\phi \approx mc^2(1-\sqrt{3}V_{th}/c-1/_{ph})$. Note that ϕ and E are no longer simply related by the ratio c/ω_p.

5. J.M. Dawson, Phys. Rev. 113, 383 (1959).

6. Berkeley Particle Data Group, Physics Letters 111B, "Review of Particle Properties", p. 39-41 (22 Apr. 1982); see also B. Montague, Proc. of Workshop on Novel Methods For Acceleration (Frascati, Italy, 1984) for discussions of smale angle scattering in plasma.

7. T. Tajima and J.M. Dawson, Phys. Rev. Lett 43, 267 (1979).

8. Laser Acceleration of Particles (Los Alamos, 1982), AIP Conference Proc. No. 91, P. Channel, Ed. (New York, 1982).

9. P. Chen, R.W. Huff, J.M. Dawson, UCLA PPG-802 (1984); P. Chen, J.M. Dawson, R.W. Huff, T. Katsouleas, Phys. Rev. Lett., 54, 693 (1985).

10. T. Katsouleas, J.M. Dawson, D. Sultana, Y.T. Yan to appear in Proc. of 13th Conference on High Energy Accelerators (TRIUMF, Canada) IEEE Trans. on Nucl. Sci (Oct 1985).

11. Landau and Lifshitz, Electrodynamics of Continous Media, Section 15, (Pergamon Press, Oxford, 1960).

12. This can be shown from a 1-D plasma model in which the electrons are treated as a series of parallel negatively charged plates in a uniform background of positive charge density $n_0 e$. In displacing an electron (or plate) by an amount x, it passes over an amount of positive charge $n_0 ex$ giving an electric field $E=4\pi n_0 ex$ at the plate. But from Poisson's Eq., $\nabla\cdot E=4\pi en_1 \sim k\cdot E$ from which $kx \approx n_1/n_0$. From the considerations in the introduction $n_1/n_0 \approx eE/m\omega_p c$ for a plasma wave at c, so $kx \approx eE/m\omega_p c$.

13. M. Rosenbluth and C.S. Liu, Phys. Rev. Lett., 29, 701 (1972); to obtain the frequency shift $3/16\ \varepsilon^2\omega_p$ from Eq. (7), one must note that if $\varepsilon \sim |\varepsilon|\cos\phi$, then $\dot{\varepsilon}^2\varepsilon \sim \sin^2\phi\cos\phi = 1/4\cos\phi$ + higher harmonics of ϕ.

14. C.M. Tang, P. Sprangle, R. Sudan, Appl. Phys. Lett, 45 (1984).

15. W. Horton and T. Tajima, "Laser Beat-Wave Accelerator and Plasma Noise", submitted to Phys. Rev. A (1985).

16. W. Mori, C. Joshi, J.M. Dawson, IEEE Trans. on Nucl. Sci., NS-30, 3244 (1983).

17. C. Joshi, W.B. Mori, T. Katsouleas, J.M. Dawson, J.M. Kindel, and D.W. Forslund, Nature 311, 525 (1984).

18. D. W. Forslund, J.M. Kindel, W. Mori, C. Joshi, and J.M. Dawson, Phys. Rev. Lett. 54, 558 (1985).

19. W. Mori, et al., private communication.

20. C. Joshi, C.E. Clayton, F.F. Chen, Phys. Rev. Lett. 48, 874 (1982).

21. C.E. Max and J. Arons, Phys. Rev. Lett. 33, 209 (1974).

22. G. Schmidt and W. Horton, see the proceedings of this conference.

23. T. Katsouleas, Ph.D. Thesis, Appendix C, UCLA PPG-769 (1984).

24. The derivation of maximum energy gain given in Ref. 7 does not make the simplifying assumption that the particle velocity is roughly c. Also, the factor 2 in Eq. (22) is obtained by assuming the particle gains energy by the amount of the wave's potential amplitude $e\phi'$ in the wave frame. Since the particle can actually gain $2e\phi'$ in going from top to bottom of the potential well, the result (22) should actually be $4\varepsilon(\omega^2/\omega_p^2)mc^2$. The latter expression is closer to the maximum particle energy observed in simulations.

25. J. Lawson, J. Allen, R. Bingham, J. Butteworth, F. Close, R. Evans, G. Rees, R. Ruth, Rutherford Appleton Laboratory Report RL 83057 (1983).

26. The question was raised by R. Ruth at the workshop as to whether or not the space charge neutralization is sufficient for focusing when accelerating injected electrons rather than accelerating particles from the tail of the plasma distribution as was the case in this simulation. The answer is probably yes because the fraction of electrons accelerated by the simulation was small and did not greatly affect the charge neutrality of the plasma, but this point still needs verification.

27. T. Katsouleas and J.M. Dawson, Phys. Rev. Lett. 51, 392 (1983).

28. D. Neuffer, Phys. Rev. Letters 53, 1026 (1984). It is also pointed out in this reference that radiation from the zeroth order surfatron motion will likely be insignificant compared to that due to fluctuations in E or B.

29. T. Katsouleas, C. Joshi, W. Mori, J.M. Dawson, F.F. Chen, Proc. 12th Int. Conf. on High Energy Accelerators, Fermilab (1983).

30. F.F. Chen, Proc. 12 SPIG, Sibenik, Yugoslavia (1984).

31. T. Katsouleas, J.M. Dawson, D. Sultana, Yi Ton Yan, to appear in Proc. 13th Conf. on High Energy Accererators, TRIUMF, Canada (1985).

32. T. Katsouleas, J.M. Dawson, and P. Chen, UCLA PPG-827 (1984).

33. T. Katsouleas, UCLA PPG 828 (1984).

34. P. Chen, J.M. Dawson (see these proceedings).